



that even if solved exactly (i.e. without space and time discretization) do violate the conservation of mass, momentum, and energy. The first step to remedy this was taken in [9], where the Galerkin condition was modified to result in a set of equations for the low-rank factors that preserve mass, momentum, and energy. It has also been shown that this can be combined with time and space discretization strategies that result in a fully discrete conservative method. However, the approach presented in this work is not robust. The main issue is that the equations for the low-rank factors are modified in such a way that they lose the property required for applying the projector splitting integrator. Realizing this, in [12], the recently proposed augmented BUG integrator [2] has been used to integrate the equations of motion forward in time. This results in a conservative scheme up to the truncation step. However, in the same work, it is shown that the truncation can be performed in a conservative way (the approach outlined there is similar to [15], where a conservative truncation is needed in the context of low-rank step truncation methods). This yields a scheme that is both conservative and robust.

In this paper we propose a different approach. We apply the augmented (also called rank-adaptive) BUG integrator [2] directly to the classic equations of motions for the low-rank factors (i.e. without ensuring that the underlying equations are conservative, as in [12]). We then apply a forward Euler time discretization to all steps of the augmented BUG integrator. It turns out that doing this results in a conservative scheme if the conservative truncation from [15, 12] is used. The reason this works is similar to [9], namely that certain basis functions required for conservation are included in the augmented basis. However, the mechanism that ensures this is different. Here, we use that the basis functions relevant for conservation are automatically included if an appropriate choice of the time discretization scheme and the truncation algorithm is made.

One advantage of this approach is that it provides a simpler conservative dynamical low-rank algorithm that, in contrast to [12], does not require us to change the Galerkin condition and the underlying equations of motion for the low-rank factors. In this work, we will provide proof that the proposed scheme is mass and momentum conservative. We will also investigate its properties numerically and show that it performs nearly identical to the scheme proposed in [12].

Let us emphasize that when we consider conservation in this paper we do not only consider (global) conservation of invariants (this can be done in a relatively straightforward way by introducing Lagrange multipliers; see, e.g., [11, 22]). Instead, our goal is to obtain numerical methods that also preserve the corresponding (local) conservation laws. In the PDE case, the latter is more important in order to improve the quality of the solution. This has been discussed in some detail in [11]. We also note that all the methods considered in the paper are based on the augmented BUG integrator and are thus naturally rank adaptive [2].

The paper is structured in the following way: After the introduction we provide a recap on kinetic equations and their conserved quantities in Section 2. Dynamical low-rank approximation is reviewed in Section 3.1 followed by a discussion of the augmented BUG integrator and the continuously conservative BUG integrator in Sections 3.2 and 3.3. In Section 4 we derive the local conservation properties of the augmented BUG integrator when using a conservative truncation step. The conservation and approximation properties of the rank-adaptive and conservative BUG integrators are shown and compared in Section 5 for kinetic problems from radiation transport and plasma physics.

## 2. Recap: Kinetic equations

Kinetic equations govern the physical processes in various applications. Commonly, they are based on a mesoscopic description of a large number of particles defined in a spatial domain  $D_x \subset \mathbb{R}^3$  moving with a velocity  $v \in D_v \subset \mathbb{R}^3$ . Besides this so-called streaming dynamics, where particles change their spatial position due to their inherent velocity, particles can change their velocity due to scattering with a background medium or with other particles. A prominent example of a kinetic equation is the radiative transfer equation

which reads

$$\partial_t f(t, x, v) + v \cdot \nabla_x f(t, x, v) + \sigma_a(x) f(t, x, v) = \int_{\mathbb{S}^2} k(x, v, v') (f(t, x, v') - f(t, x, v)) dv', \quad (1)$$

where  $D_v = \mathbb{S}^2$ ,  $\sigma_a$  is the absorption cross-section and  $k(x, v, v') = k(x, v', v)$  is the symmetric scattering kernel.

Defining the scalar flux  $\phi(t, x) := \int_{\mathbb{S}^2} f(t, x, v) dv$ , integrating (1) with respect to  $v$  gives the local conservation law

$$\partial_t \phi(t, x) + \sigma_a(x) \phi(t, x) + \nabla_x \cdot \int_{\mathbb{S}^2} v f(t, x, v) dv = 0.$$

If no absorption is present and the solution is zero at the boundary  $\partial D_x$ , integrating the local conservation law over time yields  $\frac{d}{dt} \int_{D_x} \phi(t, x) dx = 0$ , i.e., the total mass is conserved.

Another prominent example of a kinetic equation is the Vlasov equation. Assuming a constant background ion density, the Vlasov equation determines the electron density  $f(t, x, v)$  for a collisionless plasma in the electrostatic regime according to

$$\begin{aligned} \partial_t f(t, x, v) + v \cdot \nabla_x f(t, x, v) - E(f)(t, x) \cdot \nabla_v f(t, x, v) &= 0, \\ \nabla_x E(f)(t, x) &= 1 - \int_{\mathbb{R}^3} f(t, x, v) dv, \quad \nabla_x \times E(f)(t, x) = 0, \end{aligned}$$

where for dimension  $d$ , we have  $x \in D_x \subset \mathbb{R}^d$  and  $v \in D_v \subset \mathbb{R}^d$ . Commonly, one is interested in conserving mass  $M$ , momentum  $J$  and energy  $\mathcal{E}$ , given by

$$\begin{aligned} M(t) &= \int_D f(t, x, v) dx dv, \quad J(t) = \int_D v f(t, x, v) dx dv, \\ \text{and } \mathcal{E}(t) &= \frac{1}{2} \int_D v^2 f(t, x, v) dx dv + \frac{1}{2} \int_{D_x} E(t, x)^2 dx, \end{aligned}$$

where  $D = D_x \times D_v$  and  $v^2, E^2$  denote squared Euclidean norms, e.g.  $v^2 = \sum_{i=1}^d v_i^2$ . The Vlasov equation then fulfills a local conservation law for the local mass  $\rho(x)$ , momentum  $j(x)$ , and energy  $e(x)$  which are defined as

$$\begin{aligned} \rho(t, x) &= \int_{D_v} f(t, x, v) dv, \quad j(t, x) = \int_{D_v} v f(t, x, v) dv, \\ \text{and } e(t, x) &= \frac{1}{2} \int_{D_v} v^2 f(t, x, v) dv + \frac{1}{2} E(t, x)^2. \end{aligned}$$

The local conservation laws for these quantities then read

$$\begin{aligned} \partial_t \rho(t, x) + \nabla_x \cdot j(t, x) &= 0 \\ \partial_t j(t, x) + \nabla \cdot \int_{D_v} (v \otimes v) f(t, x, v) dv &= -E(t, x) \rho(t, x) \\ \partial_t e(t, x) + \nabla_x \cdot \frac{1}{2} \int_{D_v} v v^2 f(t, x, v) dv &= E(t, x) \cdot (\partial_t E(t, x) - j(t, x)). \end{aligned}$$

Conservation of mass, momentum and energy is guaranteed since  $E(1 - \rho) = \nabla_x \cdot (E \otimes E - \frac{1}{2} E^2)$  and  $\int_{D_x} E dx = 0$ .

In the following, to make the notation more general, we denote our kinetic equation as  $\partial_t f(t, x, v) = F(f(t, x, v))$ . Given a vector of  $m$  conservative basis functions  $U(v) \in \mathbb{R}^m$  and a vector of conserved

quantities  $\Phi(t, x) := \int_{D_v} f(t, x, v)U(v) dv$ , we wish to investigate dynamical low-rank time integrators which preserve the local conservation law

$$\partial_t \Phi(t, x) + \int_{\mathbb{S}^2} F(f(t, x, v))U(v) dv = 0,$$

which when integrating over the spatial domain directly yields conservation of  $\int_{D_x} \Phi(t, x) dx$  for periodic or Dirichlet boundary conditions  $f|_{\partial D_x} = 0$ .

### 3. Recap: Dynamical low-rank approximation

#### 3.1. Low-rank evolution equations

Dynamical low-rank approximation for kinetic problems revolves around the fundamental concept of expressing and evolving the solution on a manifold consisting of functions with a rank of  $r$ , which we denote as

$$\mathcal{M}_r = \left\{ f \in L^2(D_x \times D_v) : f(x, v) = \sum_{i,j=1}^r X_i(x)S_{ij}V_j(v) \text{ with invertible } S = (S_{ij}) \in \mathbb{R}^{r \times r}, \right. \\ \left. X_i \in L^2(D_x), V_j \in L^2(D_v) \text{ and } \langle X_i, X_j \rangle_x = \delta_{ij}, \langle V_i, V_j \rangle_v = \delta_{ij} \right\}.$$

Here, we denote the  $L^2$  inner product<sup>1</sup> over the spatial and velocity domain as  $\langle \cdot, \cdot \rangle_x$  and  $\langle \cdot, \cdot \rangle_v$  respectively. That is, we represent the solution through  $r$  orthonormal basis functions  $X_i$  and  $V_i$  in space and velocity respectively. The corresponding expansion coefficients are collected in the coefficient matrix  $S$ . Then, at a given time  $t$ , a low-rank solution can be written as

$$f(t, x, v) = \sum_{i,j=1}^r X_i(t, x)S_{ij}(t)V_j(t, v) := X(t, x)^\top S(t)V(t, v).$$

Here, for efficiency of notation we define  $X(t, x) = (X_i(t, x))_{i=1}^r \in \mathbb{R}^r$  and  $V(t, v) = (V_i(t, v))_{i=1}^r \in \mathbb{R}^r$ . To confine the dynamics of the solution within the low-rank manifold  $\mathcal{M}_r$ , it is necessary to identify the associated tangent space at a given position  $f$ . To ensure a bijective map between the manifold and its tangent space, we impose Gauge conditions  $\langle \dot{X}_i, X_j \rangle_x = 0$  and  $\langle \dot{V}_i, V_j \rangle_v = 0$ . Then, following [18, 10], the tangent space can be written as

$$\mathcal{T}_f \mathcal{M}_r = \left\{ \delta f \in L^2(D_x \times D_v) : \delta f(x, v) = \sum_{i,j=1}^r \delta X_i(x)S_{ij}V_j(v) + X_i(x)\delta S_{ij}V_j(v) + X_i(x)S_{ij}\delta V_j(v) \right. \\ \left. \text{with } \delta S_{ij} \in \mathbb{R}, \delta X_i \in L^2(D_x), \delta V_j \in L^2(D_v) \text{ and } \langle \delta X_i, X_j \rangle_x = 0, \langle \delta V_i, V_j \rangle_v = 0 \right\}.$$

After establishing the low-rank manifold and its associated tangent space, our objective is to find  $f(t, \cdot, \cdot) \in \mathcal{M}_r$  that satisfies two conditions: (1)  $\partial_t f(t, \cdot, \cdot) \in \mathcal{T}_f \mathcal{M}_r$ , and (2)  $\|\partial_t f(t, \cdot, \cdot) - F(f(t, \cdot, \cdot))\|_{L^2(D_x \times D_v)}$  is minimized, given a specific right-hand side  $F(f)$ . Defining the projection onto the span of  $X(t, x)$  as  $P_X$  and the projection onto the span of  $V(t, v)$  as  $P_V$ , as well as the projection onto the corresponding orthogonal spaces as  $P_X^\perp$  and  $P_V^\perp$ , the problem can be rewritten as [18]

$$\dot{S} = \langle F(f(t, \cdot, \cdot)), X(t, \cdot)V(t, \cdot)^\top \rangle_{xv} \quad (2a)$$

$$\partial_t X(t, x) = P_X^\perp \langle F(f(t, \cdot, \cdot)), V(t, \cdot)^\top \rangle_v S^{-1}(t) \quad (2b)$$

$$\partial_t V(t, v) = P_V^\perp \langle F(f(t, \cdot, \cdot)), X(t, \cdot)^\top \rangle_x S^{-\top}(t). \quad (2c)$$

<sup>1</sup>Note that when  $D_x, D_v = \mathbb{R}^d$ , the inner products  $\langle \cdot, \cdot \rangle_x$  and  $\langle \cdot, \cdot \rangle_v$  can be defined as a weighted inner product to ensure integrability of conservative basis functions  $U(v)$ .

### 3.2. The augmented BUG integrator

Standard time integrators to evolve the system (2) in time require inverting the coefficient matrix  $S$ , which when  $S$  is ill-conditioned leads to prohibitively small time step sizes. A widely used time integrator to robustly solve this system is the augmented BUG integrator [2]. Note that this integrator is also known as the rank-adaptive BUG integrator. However, we use the name augmented BUG here to not confuse the integrator with other rank-adaptive integrators. Instead of updating the factors  $X$  and  $V$  in time, it updates  $K(t, x) := X(t, x)^\top S(t)$  and  $L(t, v) := S(t)V(t, x)$  in parallel from a given time  $t_0$  to  $t_1 = t_0 + \Delta t$ . It then retrieves the time-updated basis  $X(t_1, x)$  and  $V(t_1, x)$  through a Gram-Schmidt process. To enable conservation properties and allow for rank-adaptivity, the integrator augments the time-updated basis with  $X(t_0, x)$  and  $V(t_0, x)$  and then performs a Galerkin step to update the coefficient matrix  $S$ . Lastly, the method performs a truncation step according to a user-determined tolerance parameter  $\vartheta$  to identify the rank at time  $t_1$ . In detail, starting with a rank  $r$  and the factorized solution at time  $t_0$  given by  $X^0(x)$ ,  $V^0(v)$ , and  $S^0$ , the algorithm reads as follows:

1. **K-Step:** Update and augment the basis  $X^0(x) \in \mathbb{R}^r$  to  $\widehat{X}^1(x) \in \mathbb{R}^{2r}$  by solving

$$\partial_t K(t, x) = \langle F(K(t, x)^\top V^0), V^0 \rangle_v, \quad K(t_0, x) = X^0(x)^\top S^0.$$

Compute  $\widehat{X}^1(x) \in \mathbb{R}^{2r}$  such that  $[X^0, K(t_1, x)] = \widehat{X}^1(x)^\top R$  and store  $\widehat{M} = \langle \widehat{X}^1, X^{0,\top} \rangle_x \in \mathbb{R}^{2r \times r}$ .

2. **L-Step:** Update and augment the basis  $V^0(v) \in \mathbb{R}^r$  to  $\widehat{V}^1(v) \in \mathbb{R}^{2r}$  by solving

$$\partial_t L(t, v) = \langle F(X^{0,\top} L(t, v)), X^0 \rangle_x, \quad L(t_0, v) = V^0(v)^\top S^{0,\top}.$$

Compute  $\widehat{V}^1(v) \in \mathbb{R}^{2r}$  such that  $[V^0, L(t_1, v)] = \widehat{V}^1(v)^\top \widetilde{R}$  and store  $\widehat{N} = \langle \widehat{V}^1, V^{0,\top} \rangle_v \in \mathbb{R}^{2r \times r}$ .

3. **S-step:** Update  $S^0 \in \mathbb{R}^{r \times r}$  to  $\widehat{S}^1 \in \mathbb{R}^{2r \times 2r}$  by solving

$$\dot{\widehat{S}}(t) = \left\langle F\left(\widehat{X}^{1,\top} \widehat{S}(t) \widehat{V}^1\right), \widehat{X}^1 \widehat{V}^{1,\top} \right\rangle_{xv}, \quad \widehat{S}(t_0) = \widehat{M} S^0 \widehat{N}^\top.$$

4. **Truncation:** Compute the singular value decomposition  $\widehat{S}(t_1) = \widehat{P} \widehat{\Sigma} \widehat{Q}^\top$  where  $\Sigma = \text{diag}(\sigma_j)$ . For a user-determined tolerance parameter  $\vartheta$ , choose the new rank  $r_1 \leq 2r$  as the minimal  $r_1$  such that

$$\left( \sum_{j=r_1+1}^{2r} \sigma_j^2 \right)^{1/2} \leq \vartheta$$

holds. Pick  $S^1 = \text{diag}(\sigma_1, \dots, \sigma_{r_1})$  and let  $P$  and  $Q$  contain the first  $r_1$  columns of  $\widehat{P}$  and  $\widehat{Q}$ , respectively. Then choose  $X^1(x) = \widehat{X}^1(x)^\top P \in \mathbb{R}^{r_1}$  and  $V^1(v) = \widehat{V}^1(v)^\top Q \in \mathbb{R}^{r_1}$ .

Then, the factorized solution at time  $t_1$  with rank  $r_1$  is given as  $X^1(x)$ ,  $V^1(v)$ , and  $S^1$ . By successively using the above algorithm, the solution can then be evolved to a given time  $t_n$ .

The augmented BUG integrator possesses several beneficial properties compared to the fixed-rank BUG integrator of [4]. Perhaps most importantly, besides the ability to achieve rank-adaptivity, the augmented BUG integrator fulfills an important conservation property. Unlike the fixed-rank BUG integrator, the rank-adaptive version does not introduce an error when constructing  $\widehat{S}(t_0)$  in the  $S$  step equation [2, Lemma 1]: Let  $f_0 = X^{0,\top} S^0 V^0$  and  $\widehat{f}_0 = \widehat{X}^{1,\top} \widehat{S}(t_0) \widehat{V}^1$ . Then,  $f_0 = \widehat{f}_0$ , which is due to the fact that the old basis at time  $t_0$  is included in the augmented basis used in the Galerkin step. It has been shown in [2] that this property enables norm conservation as well as energy conservation for Schrödinger and Hamiltonian systems. Invariants of kinetic systems such as mass are however not conserved by the augmented BUG integrator. We will show in this paper that the augmentation step guarantees the conservation of invariants up to a user-determined tolerance parameter.

### 3.3. The continuously conservative BUG integrator of [12]

The conservative integrator of [12] is constructed to preserve local conservation laws, specifically for the Vlasov equation, however, the strategy extends to other kinetic problems. One core building block is to evolve  $V(t, v)$  such that basis functions  $U(v) \in \mathbb{R}^m$  which are important for conservation are spanned by the basis. Following [9], the DLRA evolution equations (2) are modified to preserve the basis directions  $U(v)$ . Denoting  $W_p(t, v) = V_p(t, v)$  for  $m < p \leq r$ , the DLRA evolution equations with  $f_r(t, x, v) = X(t, x)^\top S(t) V(t, v)$  change to

$$\sum_{i=1}^r \dot{X}_i S_{ik} = \langle V_k, F(f_r) \rangle_v - \sum_{i=1}^r X_i \dot{S}_{ik}, \quad 1 \leq k \leq r \quad (3a)$$

$$\sum_{i=1}^r \sum_{p=m+1}^r S_{iq} S_{ip} \dot{W}_p = \sum_{i=1}^r S_{iq} \langle S_{iq} \langle X_i, F(f_r) \rangle_x \rangle - \sum_{i,l=1}^r S_{iq} \dot{S}_{il} V_l, \quad m+1 \leq q \leq r \quad (3b)$$

$$\dot{S}_{kl} = \langle X_k V_l, F(f_r) \rangle_{xv}, \quad 1 \leq k, l \leq r. \quad (3c)$$

Here, we use index notation to precisely define the ranges of sums and leave out dependencies on the phase space for better readability. While this system has been solved through a non-robust time integration scheme in [9], the BUG integrator has been employed in [12] to obtain stability independent of the curvature of the low-rank manifold. To remove the projection error of the  $S$  step in the fixed-rank integrator, the augmentation strategy of [2, Lemma 1] is used. That is, the basis at the previous time step  $t_0$  is included in the Galerkin step to remove the projection error of the initial condition for the Galerkin step.

Moreover, the authors add the basis  $\nabla X^0$  in order to be able to represent the local conservation law  $\partial_t \rho + \nabla \cdot j = 0$  exactly. That  $\nabla \cdot j$  lies in the approximation space then also implies that we can represent the local conservation laws for momentum and energy exactly (on the continuous level). However, what the authors in [12] did not realize is that there is no need to explicitly add  $\nabla X^0$  to the basis. To see this it is sufficient to consider the local conservation law for mass. In the K-step

$$\nabla \cdot j = -\partial_t \rho = \int \partial_t f \, dv = \int F(f) \, dv = \langle F(f), 1 \rangle_v$$

Thus,  $\nabla \cdot j$  is already ensured to lie in  $\text{span}\{X^1\}$  as it is ensured that  $1$  lies in  $\text{span}\{X^0\}$ . This has two important consequences. First, adding the additional basis functions results in a larger space and thus increased computational cost. Second, in some situations, the fact that we add redundant basis functions to the orthogonalization procedure can result in increased round-off error. We thus, will denote the variant of the algorithm by *continuously conservative integrator* which does not add  $\nabla X^0$  to the basis.

The full algorithm reads as follows: Starting with a rank  $r$  and the factorized solution at time  $t_0$  given by  $X^0(x)$ ,  $V^0(v)$ , and  $S^0$ , we define  $f_r^0 = X^{0,\top} S^0 V^{0,\top}$ . Moreover,  $\tilde{S} := (S_{ij})_{i=1, j=m+1}^r \in \mathbb{R}^{r \times r-m}$  and  $W^0(v) = (V_i^0(v))_{i=m+1}^r$ . Then, the algorithm performs the following steps:

1. **K-Step:** Update and augment the basis  $X^0(x) \in \mathbb{R}^r$  to  $\hat{X}^1(x) \in \mathbb{R}^{2r}$  by solving

$$K^1(x) = K^0(x) + \Delta t \langle F(f_r^0), V^0 \rangle_v, \quad K^0(x) = X^0(x)^\top S^0.$$

Compute  $\hat{X}^1(x) \in \mathbb{R}^{2r}$  such that  $[X^0, K^1] = \hat{X}^1(x)^\top R$  and store  $\hat{M} = \langle \hat{X}^1, X^{0,\top} \rangle_x \in \mathbb{R}^{2r \times r}$ .

2. **L-Step:** Update and augment the basis  $V^0(v) \in \mathbb{R}^r$  to  $\hat{V}^1(v) \in \mathbb{R}^{2r-m}$  by solving

$$L^1(v) = L^0(v) + \Delta t \left\langle F(f_r^0), X^0 \tilde{S}^0 \right\rangle_x - \Delta t \left\langle F(f_r^0), \tilde{S}^{0,\top} X^0 V^{0,\top} \right\rangle_{xv} V^0, \quad L^0(v) = W^0(v)^\top \tilde{S}^{0,\top} \tilde{S}^0.$$

Compute  $\hat{V}^1(v) \in \mathbb{R}^{(2r-m)}$  such that  $[V^0, L^1] = \hat{V}^1(v)^\top \tilde{R}$  and store  $\hat{N} = \langle \hat{V}^1, V^{0,\top} \rangle_v \in \mathbb{R}^{(2r-m) \times r}$ .

3. **S-step:** Update  $S^0 \in \mathbb{R}^{r \times r}$  to  $\widehat{S}^1 \in \mathbb{R}^{2r \times (2r-m)}$  by solving

$$\widehat{S}^1 = \widehat{S}^0 + \Delta t \left\langle F(f_r^0), \widehat{X}^1 \widehat{V}^{1,\top} \right\rangle_{xv}, \quad \widehat{S}(t_0) = \widehat{M} S^0 \widehat{N}^\top.$$

4. **Truncation:** Perform a conservative truncation given a user-determined tolerance parameter  $\vartheta$ .

The conservative truncation step preserves conserved quantities. The core idea works as follows:

1. Split  $K = \widehat{X}^{1,\top} \widehat{S}^1$  into  $K = [K_{\text{cons}}, K_{\text{rem}}]$  where  $K_{\text{cons}} \in \mathbb{R}^m$  and  $K_{\text{rem}} \in \mathbb{R}^{3r-m}$ . Factorize into

$$K_{\text{rem}} = \widehat{X}_{\text{rem}} \widehat{S}_{\text{rem}}, \quad K_{\text{cons}} = X_{\text{cons}} S_{\text{cons}}.$$

2. Truncate  $\widehat{S}_{\text{rem}}$  according to the truncation step in [2] leading to  $S_{\text{rem}} = P \Sigma Q^\top \in \mathbb{R}^{(r_1-m) \times (r_1-m)}$  and basis functions  $X_{\text{rem}} = \widehat{X}_{\text{rem}}^\top P \in \mathbb{R}^{r_1-m}$ ,  $V_{\text{rem}} = Q^\top \widehat{W} \in \mathbb{R}^{r_1-m}$ , where  $\widehat{W} = (\widehat{V}_i^1)_{i=m+1}^{2r}$ .

3. Add conserved quantities with  $X^{1,\top} R = [X_{\text{cons}}, X_{\text{rem}}]$ ,  $V^1 = [U, V_{\text{rem}}]$  and

$$S^1 = R \begin{pmatrix} S_{\text{cons}} & 0 \\ 0 & S_{\text{rem}} \end{pmatrix}.$$

As remarked in [12], the truncation step for the Vlasov system can be performed to either control the error in the kinetic density  $f$  by cutting singular values in the coefficient matrix, or by cutting singular values such that the energy error is controlled. That is,

$$\|\widehat{e} - e^{r_1}\| \leq \vartheta,$$

where  $\widehat{e}$  is the electric energy with augmented basis and  $e^{r_1}$  denotes the electric energy truncated to a rank  $r_1$ . This truncation can be beneficial, since for Vlasov equations one is usually not interested in the particle density  $f$  but in the electric energy  $e$ .

Note that the augmented BUG integrator [2] is very similar to the continuously conservative BUG integrator. Besides the truncation algorithm, the integrators primarily differ in that the continuously conservative BUG integrator solves system (3) instead of (2). Note that the advantage of the continuously conservative integrator is that compared to the augmented BUG integrator, the  $S$  step is performed for a reduced number of basis functions in velocity which can yield a reduction in run time when the number of conserved quantities  $m$  is sufficiently big. However, these reduced costs in the  $S$  step come with an increased number of operations in the  $L$  step since additional flux terms need to be computed. In our numerical experiments, we observed that both approaches exhibit comparable runtimes.

We remark that the continuously conservative integrator can in principle be combined with higher order time integration methods. However, it needs to be noted that currently no high order time integrators that are robust with respect to the curvature of the low-rank manifold exist.

#### 4. Local conservation of the augmented BUG integrator

In the following, we demonstrate that the augmented BUG integrator of [2] fulfills local conservation. That is, defining  $\phi_S(t_{n+1}, x) := \langle \widehat{X}(x)^{n+1,\top} \widehat{S}^{n+1} U(v) \rangle_v$  and  $\phi_S(t_n, x) := \langle \widehat{X}(x)^{n,\top} \widehat{S}^n U(v) \rangle_v$ , the scheme fulfills the local conservation law

$$\phi_S(t_{n+1}, x) = \phi_S(t_n, x) + \Delta t \langle F(f^n), U \rangle_v$$

when a conservative truncation step, e.g., [12, 15] is used. Hence, the truncation step ensures that if the vector of  $m$  conserved basis functions  $U(v) \in \mathbb{R}^m$  lies in the augmented basis, i.e.,  $\sum_{i=1}^{2r} \langle U(v), \widehat{V}_i^1(v) \rangle_v \widehat{V}_i^1(v) = U(v)$ , then after the truncation we have  $\sum_{i=1}^{2r} \langle U(v), V_i^1(v) \rangle_v V_i^1(v) = U(v)$ . Without such a truncation step, conservation is preserved up to the tolerance parameter  $\vartheta$ .

Moreover, to derive conservation, we choose a forward Euler step to discretize all substeps of the integrator in time. Hence, for  $f^n(x, v) := X^{n,\top} S^n V^n$  we have at a given time step  $n$

$$K^{n+1}(x) = K^n(x) + \Delta t \langle F(f^n(x, \cdot)), V^n \rangle_v, \quad (4a)$$

$$L^{n+1}(x) = L^n(x) + \Delta t \langle F(f^n(\cdot, v)), X^n \rangle_x, \quad (4b)$$

$$\widehat{S}^{n+1} = \widehat{S}^n + \Delta t \left\langle F(f^n), \widehat{X}^{n+1} \widehat{V}^{n+1,\top} \right\rangle_{x,v}. \quad (4c)$$

Here, we have used the fact that by the augmentation step the initial condition is preserved, that is,  $f^n = \widehat{X}^{n+1,\top} \widehat{S}^n \widehat{V}^{n+1}$ .

First, let us note that if  $U(v)$  is spanned by  $V^n(v)$ , then it will also be spanned by  $\widehat{V}^{n+1}(v)$ . This directly follows from the augmentation step  $[V^n, L^{n+1}(v)] = \widehat{V}^{n+1}(x)^\top \widetilde{R}$  which forces  $V^n(v)$  to lie in the basis  $\widehat{V}^{n+1}(v)$ . Hence,

$$\sum_{i=1}^{2r} \langle U(v), \widehat{V}_i^{n+1}(v) \rangle_v \widehat{V}_i^{n+1}(v) = \sum_{i=1}^r \langle U(v), V_i^n(v) \rangle_v V_i^n(v) = U(v).$$

Together with the conservative truncation step we then directly know that

$$U(v) = \sum_{i=1}^{2r} \langle U(v), \widehat{V}_i^{n+1}(v) \rangle_v \widehat{V}_i^{n+1}(v) = \sum_{i=1}^{r_{n+1}} \langle U(v), V_i^{n+1}(v) \rangle_v V_i^{n+1}(v).$$

Hence if  $U(v)$  is spanned by the basis at time  $t_0 = 0$ , we know that  $U(v)$  remains in the basis at all subsequent timesteps  $t_n$ .

Second, let us note that  $\langle F(f^n(x, \cdot)), U_i(v) \rangle_v$  for  $i \leq m$  lies in the range of our basis  $\widehat{X}^{n+1}$ : Note that

$$\langle F(f^n(x, \cdot)), U(v) \rangle_v = \sum_i \langle F(f^n(x, \cdot)), \langle U(v), V_i^n(v) \rangle_v V_i^n(v) \rangle_v = \frac{1}{\Delta t} \sum_i (K_i^{n+1}(x) - K_i^n(x)) \langle U(v), V_i^n(v) \rangle_v.$$

Since by the augmentation step  $[X^n(x), K^{n+1}(x)] = \widehat{X}^{n+1}(x)^\top R$  the term  $K_i^{n+1}(x) - K_i^n(x)$  is spanned exactly by the augmented basis  $\widehat{X}^{n+1}(x)$  we know that

$$\langle F(f^n(x, \cdot)), U(v) \rangle_v = \langle \langle F(f^n(x, \cdot)), U(v) \rangle_v, \widehat{X}^{n+1,\top} \rangle_x \widehat{X}^{n+1}(x).$$

Lastly, we derive a discrete update equation from  $\phi_S(t_n, x) = \langle \widehat{X}(x)^{n+1,\top} \widehat{S}^n, U(v) \rangle_v$  to  $\phi_S(t_{n+1}, x) = \langle \widehat{X}(x)^{n+1,\top} \widehat{S}^{n+1}, U(v) \rangle_v$ . Multiplication of the  $S$ -step (4c) with  $\widehat{X}^{n+1}(x)$  and  $\langle \widehat{V}_i^{n+1}, U^\top \rangle_v$  gives

$$\begin{aligned} \phi_S(t_{n+1}, x) &= \phi_S(t_n, x) + \Delta t \sum_{i=1}^{2r} \widehat{X}^{n+1}(x)^\top \left\langle F(f^n), \widehat{X}^{n+1} \widehat{V}^{n+1,\top} \right\rangle_{x,v} \langle \widehat{V}_i^{n+1}, U^\top \rangle_v \\ &= \phi_S(t_n, x) + \Delta t \sum_{i=1}^{2r} \left\langle \langle F(f^n), U \rangle_v, \widehat{X}^{n+1,\top} \right\rangle \widehat{X}^{n+1}(x) \\ &= \phi_S(t_n, x) + \Delta t \langle F(f^n), U \rangle_v. \end{aligned}$$

The augmented BUG integrator is hence conservative when using a forward Euler time discretization in the  $S$  step combined with a conservative truncation. We call this method the *conservative augmented BUG integrator*. The full algorithm reads as follows: Starting with a rank  $r$  and the factorized solution at time  $t_0$  given by  $X^0(x)$ ,  $V^0(v)$ , and  $S^0$ , we define  $f_r^0 = X^{0,\top} S^0 V^{0,\top}$ . Then, the algorithm performs the following steps:



1. **K-Step:** Update and augment the basis  $X^0(x) \in \mathbb{R}^r$  to  $\widehat{X}^1(x) \in \mathbb{R}^r$  by solving

$$K^1(x) = K^0(x) + \Delta t \langle F(f_r^0), V^0 \rangle_v, \quad K^0(x) = X^0(x)^\top S^0.$$

Compute  $\widehat{X}^1(x) \in \mathbb{R}^{2r}$  such that  $[X^0, K^1] = \widehat{X}^1(x)^\top R$  and store  $\widehat{M} = \langle \widehat{X}^1, X^{0,\top} \rangle_x \in \mathbb{R}^{2r \times r}$ .

2. **L-Step:** Update and augment the basis  $V^0(v) \in \mathbb{R}^r$  to  $\widehat{V}^1(v) \in \mathbb{R}^{2r}$  by solving

$$L^1(v) = L^0(v) + \Delta t \langle F(f_r^0), X^0 \rangle_x, \quad L^0(v) = V^0(v)^\top S^{0,\top}.$$

Compute  $\widehat{V}^1(v) \in \mathbb{R}^{2r}$  such that  $[V^0, L^1] = \widehat{V}^1(v)^\top \widetilde{R}$  and store  $\widehat{N} = \langle \widehat{V}^1, V^{0,\top} \rangle_v \in \mathbb{R}^{2r \times r}$ .

3. **S-step:** Update  $S^0 \in \mathbb{R}^{r \times r}$  to  $\widehat{S}^1 \in \mathbb{R}^{2r \times 2r}$  by solving

$$\widehat{S}^1 = \widehat{S}^0 + \Delta t \left\langle F(f_r^0), \widehat{X}^1 \widehat{V}^{1,\top} \right\rangle_{xv}, \quad \widehat{S}(t_0) = \widehat{M} S^0 \widehat{N}^\top.$$

4. **Truncation:** Perform a conservative truncation given a user-determined tolerance parameter  $\vartheta$ .

Let us remark two important details:

1. Note that we assume existence of  $\int \phi(v) dv$ . When  $\phi(v)$  does not have bounded support, a weighted integral can be defined according to [9] to ensure existence.
2. To use the conservative truncation as described in Section 3.3, it is important to perform the augmentation as described in the above algorithm. That is we augment according to  $[V^0, L^1] = \widehat{V}^1(v)^\top \widetilde{R}$  instead of  $[L^1, V^0] = \widehat{V}^1(v)^\top \widetilde{R}$ . In this case, we ensure that the conservative basis  $U(v)$  is stored as the first  $m$  basis functions in  $\widehat{V}^1(v)$ .

We emphasize again that the above described conservative augmented BUG integrator is a slight variation of the BUG integrator of [2], where the truncation step is changed and the integrator is applied to the conservative system.

## 5. Numerical results

In the following, we compare the continuously conservative BUG integrator of [12] to the conservative augmented BUG integrator in several test cases from radiation transport and plasma physics. All numerical experiments can be reproduced with the openly available source code<sup>2</sup>

### 5.1. Results for radiation transport

In the first section of numerical results, we investigate two radiation transport test cases and compare the continuously conservative BUG integrator with the conservative augmented BUG integrator. Further, we investigate the difference between the continuously conservative integrator with and without advection terms in the augmented basis.

#### 5.1.1. Planesource testcase

In this numerical example, the radiation transport equation (1) in a one-dimensional slab geometry setting. In this case, the solution is projected onto a one-dimensional domain such that  $x \in [a, b]$  and  $v \in [-1, 1]$ . The initial condition is a Gaussian with a standard deviation of  $\sigma_{\text{IC}} = 3 \cdot 10^{-2}$  and is independent of  $\mu$ , meaning that particles fly into all possible directions. In slab geometry, the radiation transport equation (1) then becomes

$$\begin{aligned} \partial_t f + v \partial_x f + \sigma_s f &= \frac{\sigma_s}{2} \int_{-1}^1 f dv, \\ f(t=0, x, v) &= \frac{1}{\sqrt{2\pi\sigma_{\text{IC}}}} \exp\left(-\frac{x^2}{2\sigma^2}\right). \end{aligned}$$

<sup>2</sup><https://github.com/JonasKu/Publication-Conservation-properties-of-the-augmented-basis-update-Galerkin-integrator>

Here, we use isotropic scattering, that is the scattering kernel is independent of  $v$  and we choose  $k(x, v', v) = \sigma_s = 1$  as well as  $\sigma_a = 0$ . This test case is known as the planesource benchmark test [14] and is widely used since an analytic solution to this problem can be determined. Furthermore, due to the moderate scattering strength and the fact that particles move in all possible directions, this test case is challenging for various computational methods and is often used to demonstrate deficiencies in given numerical schemes. As we can see in Figure 1a the conservative augmented BUG and continuously conservative BUG integrators yield satisfactory solution behavior and show errors which for this test case are generally considered small. However, both methods require a relatively high rank which is depicted in Figure 1b. Here, we choose a tolerance parameter  $\vartheta = \bar{\vartheta} \cdot \|\hat{S}^1\|$  with  $\bar{\vartheta} = 10^{-2}$ , following the choice in [2]. As shown in Figure 2c, the

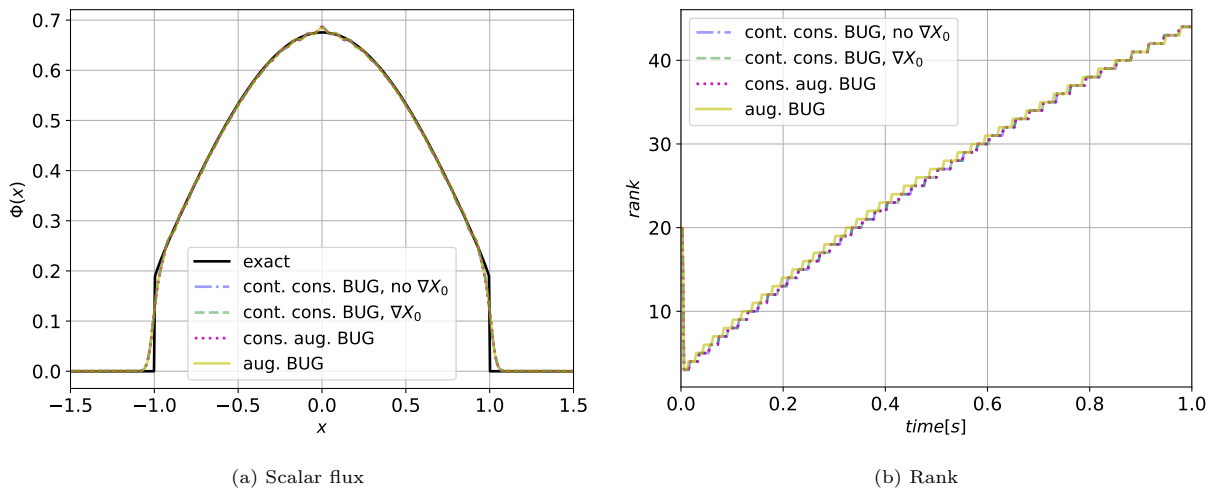


Figure 1: Comparison of the continuously conservative integrator (cont. cons. BUG) of [12], the conservative augmented BUG integrator and the standard augmented BUG integrator of [2] for the line source test case at  $t_{\text{end}} = 1$ . All integrators are rank adaptive with threshold  $\vartheta = \bar{\vartheta} \|\hat{S}^1\|$  with  $\bar{\vartheta} = 10^{-2}$ . All methods exhibit similar rank dynamics (right) and solution behavior (left).

continuously conservative BUG integrator shows an increased error in the total mass conservation, if the basis is augmented by  $\nabla X^0$ . Adding  $\nabla X^0$  in the augmentation step will not provide new information, since these basis directions are already represented in  $\text{span}\{X^0, K^1\}$ . Therefore, the QR decomposition will pick randomly chosen basis functions that are highly irregular and lead to increased rounding errors. Removing the redundant information in the conservative integrator, that is leaving out the augmentation with  $\nabla X^0$  will fix this issue. The resulting mass error is shown in Figure 2a. Note that this integrator is the conservative augmented BUG integrator applied to the system (3).

### 5.1.2. Linesource testcase

Next, we examine the radiation transport equation in the context of the line source benchmark [13]. This scenario involves a particle pulse distributed uniformly in all directions along the z-axis. The initial particle pulse is represented by a Gaussian distribution with a standard deviation of  $\sigma_{\text{IC}} = 0.03$ . As time progresses, the particles interact with a background medium that has an isotropic scattering kernel  $k(x, v, v') = \frac{\sigma_s}{4\pi}$  with  $\sigma_s = 1$ . Absorption is not present, that is,  $\sigma_a = 0$ . Then, for  $v \in \mathbb{S}^2$  and  $x \in \mathbb{R}^2$  the radiation transport equation reads

$$\partial_t f + v_1 \partial_{x_1} f + v_2 \partial_{x_2} f + \sigma_s f = \frac{\sigma_s}{4\pi} \int_{\mathbb{S}^2} f dv,$$

$$f(t = 0, x, v) = \frac{1}{4\pi \sigma_{\text{IC}}^2} \exp\left(-\frac{\|x\|^2}{4\sigma_{\text{IC}}^2}\right).$$

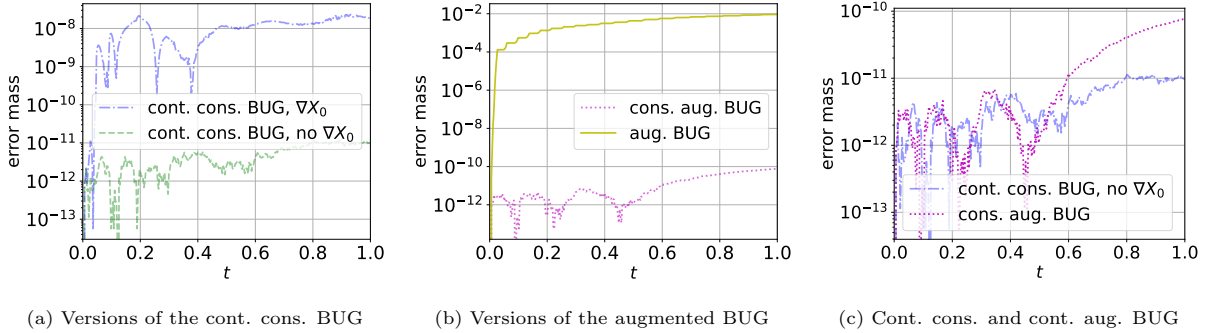


Figure 2: Mass error comparison of the continuously conservative BUG integrator (cont. cons. BUG) of [12], the conservative augmented BUG integrator (cons. aug. BUG) and the standard augmented BUG integrator (aug. BUG) of [2] for the line source test case.  $\vartheta = \bar{\vartheta} \|\hat{S}^1\|$  with  $\bar{\vartheta} = 10^{-2}$ ,  $t_{\text{end}} = 1$ . In a) it is apparent that augmentation of the basis with  $\nabla X^0$  introduces round-off errors. In b) one sees, that the non-conservative version of the BUG integrator introduces significant errors in the conserved quantity. In c) we see, that the mass error of both the cont. cons. and cons. aug. BUG integrators are within machine precision.

The scalar flux  $\phi(t, x) := \int_{\mathbb{S}^2} f(t, x, v) dv$  of the analytic solution to this equation at time  $t = 1$  is depicted in Figure 3a. Here, particles have moved into all possible directions on the sphere and are projected onto the two-dimensional spatial domain. Similar to the planesource test, This test case is particularly challenging for numerical simulations and is commonly used to lay bare deficiencies and weaknesses of computational methods. More specifically, modal approximations tend to lead to heavy oscillations while nodal approximations show spurious ray effects, that is, unwanted numerical artifacts that significantly reduce the solution quality.

In our numerical simulation, we use  $250^2$  spatial cells to represent the spatial domain and  $31^2$  modal coefficients to represent the directional basis. The chosen tolerance for the truncation step of the integrators is set to  $\vartheta = \bar{\vartheta} \|\hat{S}^1\|$  with  $\bar{\vartheta} = 5 \cdot 10^{-2}$ . Similar to conventional numerical methods, dynamical low-rank approximation struggles to approximate this test case efficiently, since a large rank is required. The resulting scalar flux for the augmented BUG integrator with adaptive rank is depicted in Figure 3b. We see oscillatory artifacts which are expected when using  $31^2$  directional modes to represent the basis. The continuously conservative BUG with and augmentation by the advection term are depicted in Figures 3c and 3d which show a similar solution quality. A comparison of all three methods is depicted in Figure 4a which shows a horizontal cut through the spatial domain at  $y = 0$ .

In general, considering the challenging structure of this test case, the approximation results show a satisfactory solution quality. This solution quality is however reached with significantly increased ranks, which are depicted in Figure 4b. As observed in Figure 5a, just as for the one-dimensional test case, the continuously conservative BUG integrator does not show exact conservation which is most likely caused by highly oscillatory basis functions that appears due to the redundant information that is added when augmenting with  $\nabla X^0$ . The conservative augmented BUG integrator for both the conservative system (3) and the original system (2) yield conservation up to machine precision. The computational costs of the methods are compared in Table 1, where we see that the rank adaptive BUG integrators decrease runtime by 20%, compared to the conservative BUG, due to the smaller number of basis augmentations.

## 5.2. Results for plasma physics

In this section of numerical results, we investigate three test cases for plasma physics. The continuously conservative BUG integrator [12] is compared to the conservative BUG integrator and to the non-conservative augmented BUG integrator of [2].

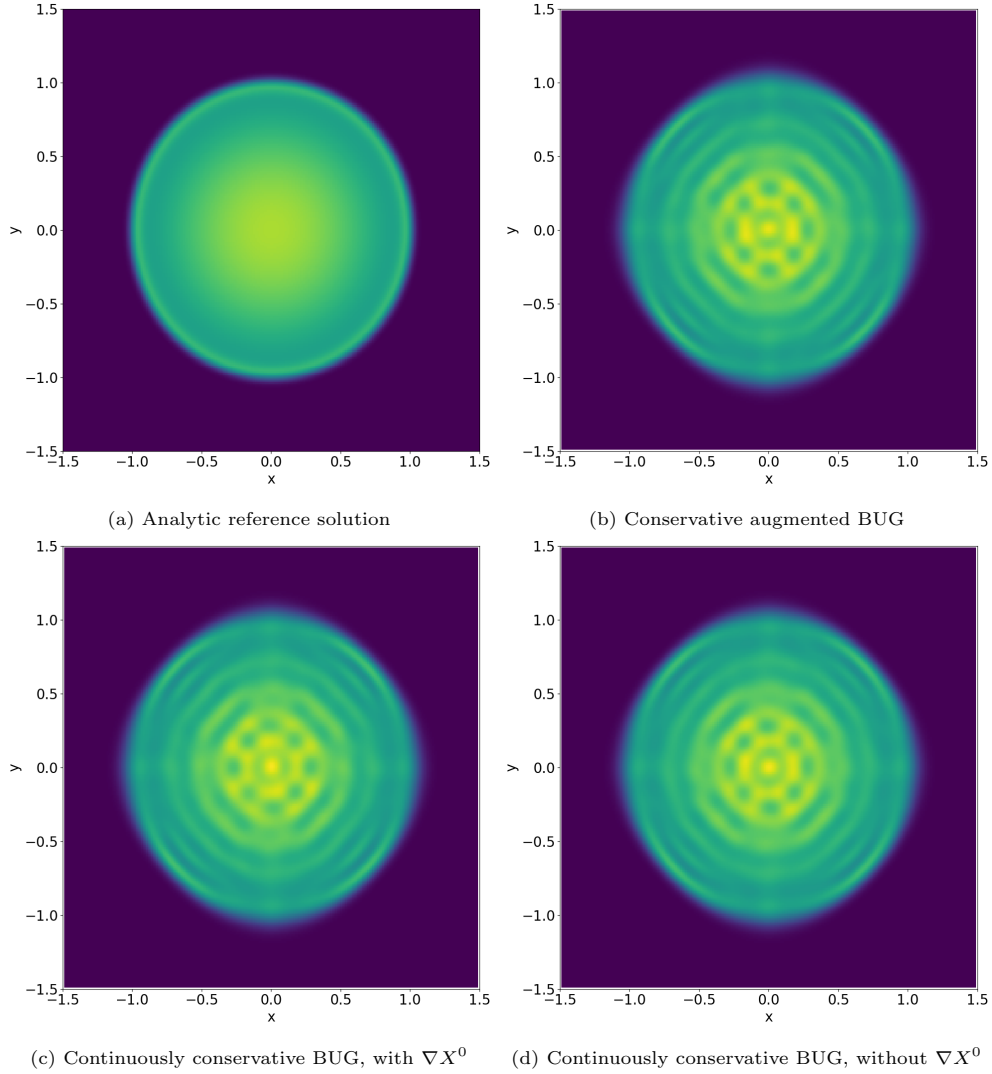


Figure 3: Linesource simulation using the conservative augmented BUG integrator (b) and the continuously conservative BUG integrator with (c) and without (d) basis augmentation by  $\nabla X^0$ . The truncation threshold is given by  $\vartheta = \bar{\vartheta} \|\widehat{S}^1\|$  with  $\bar{\vartheta} = 5 \cdot 10^{-2}$ ,  $t_{\text{end}} = 1$ .

Table 1: Computational cost comparison of the presented methods. The additional costs due to the increased number of augmentations show higher run-time for the conservative BUG integrator compared with the rank adaptive versions.

Method	mean simulation time [s]	
	Planesource	Linesource
continuously conservative BUG, 3.3	9.509	508
augmented BUG, 3.2	6.292	395

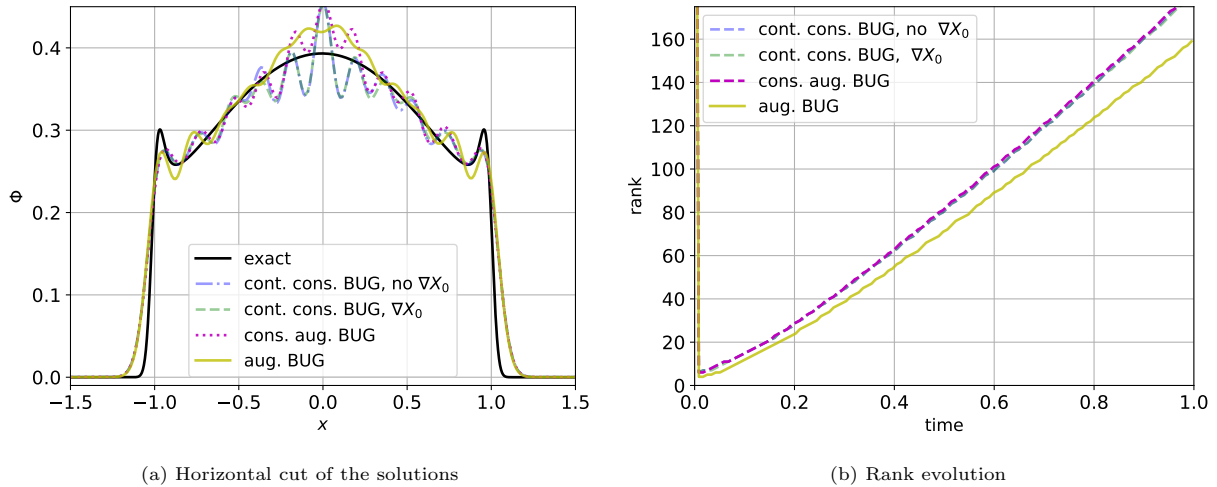


Figure 4: Solution mass across a horizontal cut through the domain (a) and rank evolution (b) of the cont. cons. BUG integrator [12] with and without advection and the conservative augmented BUG Integrator [2] for the linesource test case.  $\vartheta = \bar{\vartheta} \|\hat{S}^1\|$  with  $\bar{\vartheta} = 0.05$ ,  $t_{\text{end}} = 1$ . All integrators lead to similar rank evolution.

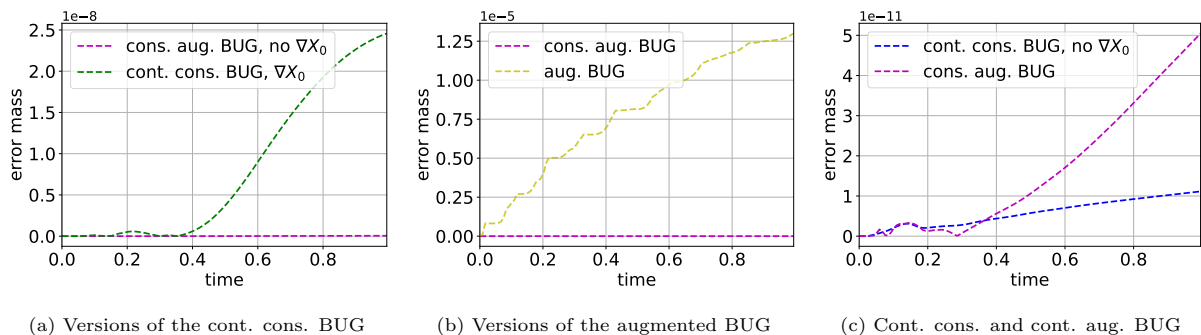


Figure 5: Mass error comparison of the continuously conservative integrator (cont. cons. BUG) of [12] and the conservative and non-conservative augmented BUG integrator of [2] for the line source test case.  $\vartheta = \bar{\vartheta} \|\hat{S}^1\|$  with  $\bar{\vartheta} = 0.05$ ,  $t_{\text{end}} = 1$ .

### 5.2.1. Linear Landau damping

Following the numerical experiments in [12], we investigate the linear Landau damping problem which uses an initial condition of the form

$$f(t=0, x, v) = (1 + \alpha \cos(kx)) \frac{\exp(-v^2/2)}{\sqrt{2\pi}}$$

with parameters  $\alpha = 10^{-2}$  and  $k = 0.5$ . The spatial domain  $D_x = [0, 4\pi]$  as well as the computational domain for velocity  $D_v = [-6, 6]$  is discretized using 128 grid points in each domain. The time step size is  $\Delta t = 10^{-3}$  and we use a fixed rank of 5. That is, the rank is always cut to  $r = 5$  in the truncation step as done in [12, Section 6.1]. We observe a similar error behavior for both conservative methods in Figure 6b-d. The most notable difference is observed in the energy error. However, this error is of the same order of magnitude for both methods. Moreover, we observe that both methods preserve energy and momentum up to machine precision. The electric energy profiles in Figure 6a agree well with each other and show the characteristic profiles for linear Landau damping. The non-conservative, standard BUG integrator on the other hand shows much larger errors, especially in the mass and momentum variable.

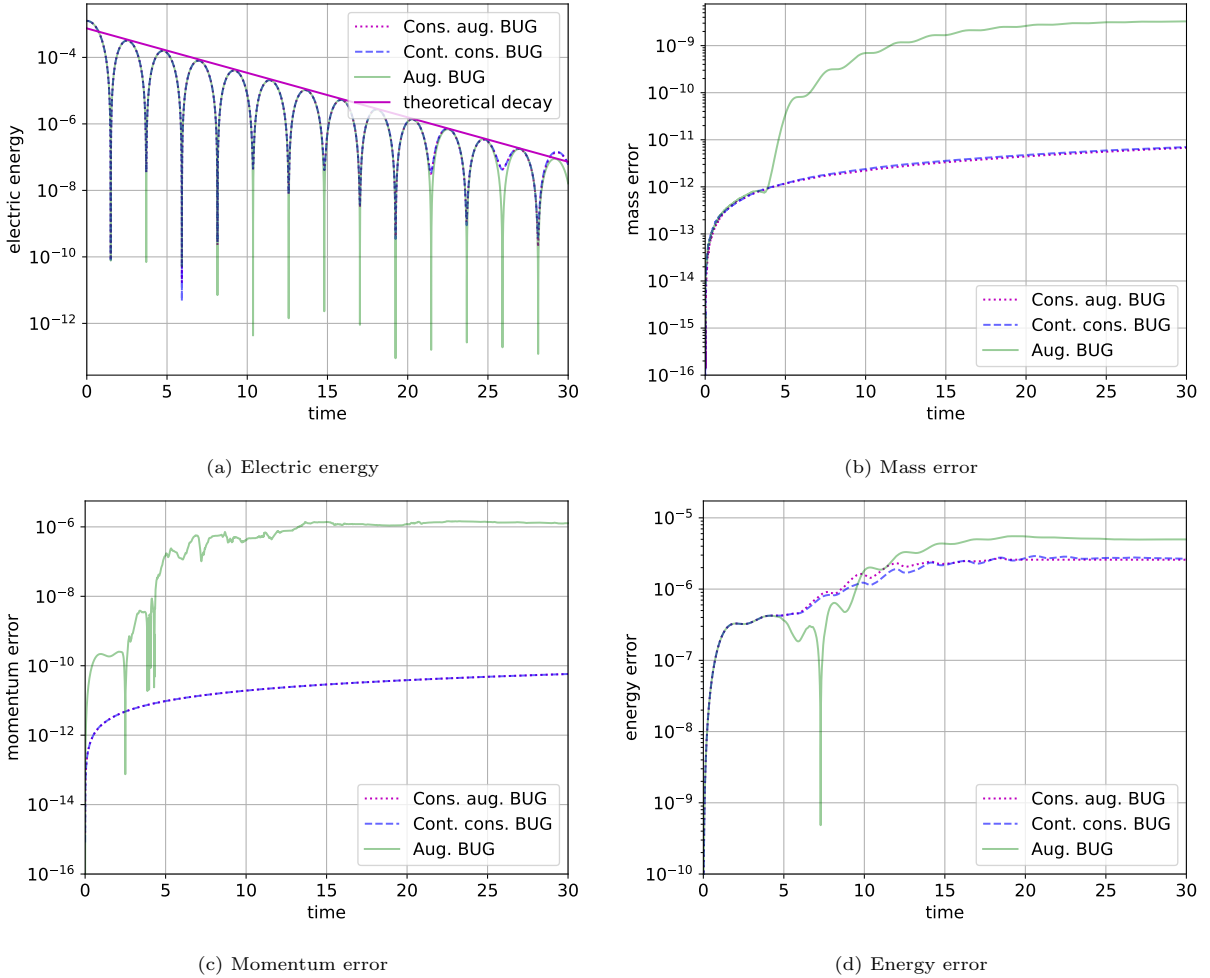


Figure 6: Comparison of the continuously conservative integrator (cont. cons. BUG) of [12], the conservative augmented BUG integrator and the standard augmented BUG integrator of [2] for the linear Landau damping test case.

### 5.2.2. Non-linear Landau damping

Similar to the previous numerical experiment, we investigate the Landau damping with the initial condition

$$f(t = 0, x, v) = (1 + \alpha \cos(kx)) \frac{\exp(-v^2/2)}{\sqrt{2\pi}}$$

where now we choose parameters  $\alpha = 0.5$  and  $k = 0.5$ . Due to the increase in  $\alpha$ , the problem will create strong non-linear effects leading to a more complicated solution structure. As in the previous test case, the spatial domain  $D_x = [0, 4\pi]$  as well as the computational domain for velocity  $D_v = [-6, 6]$  is discretized using 128 grid points in each domain. The time step size is  $\Delta t = 10^{-3}$  and we use an increased fixed rank of 25. That is, the rank is always cut to  $r = 25$  in the truncation step as done in [12, Section 6.2]. As before, a similar error behavior is observed for both conservative methods in Figure 7b-d. While both methods preserve mass and momentum up to machine precision, the energy is not preserved and the error is showing the same order of magnitude for both methods. Again, the standard augmented BUG integrator fails to conserve momentum and mass up to machine precision. The electric energy profiles in Figure 7a agree well with each other and show the characteristic profiles of this test case.

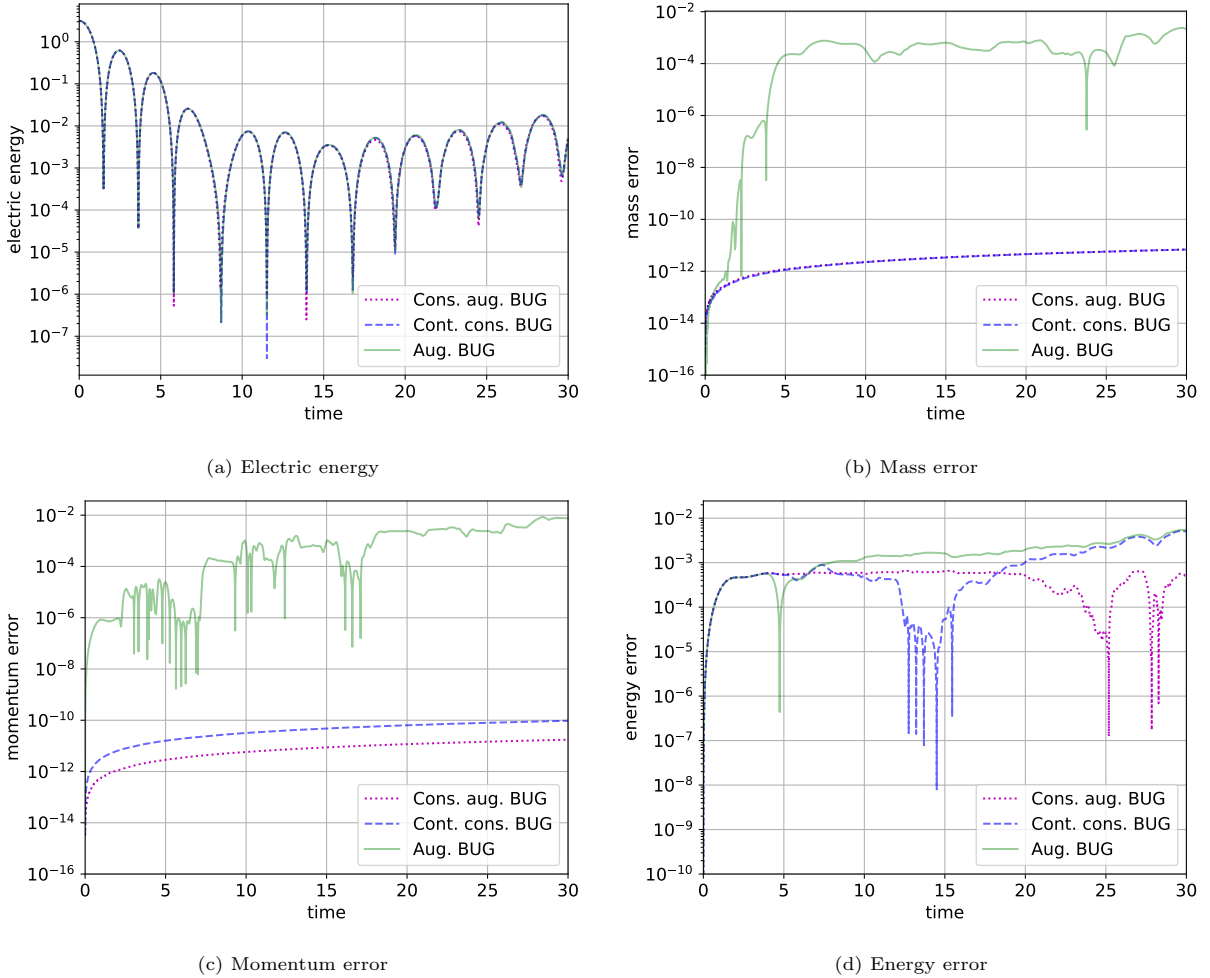


Figure 7: Comparison of the continuously conservative integrator (cont. cons. BUG) of [12], the conservative augmented BUG integrator and the standard augmented BUG integrator of [2] for the non-linear Landau damping test case.

### 5.2.3. Two stream instability

Following the numerical experiments in [12], we investigate the two-stream instability which uses an initial condition of the form

$$f(t = 0, x, v) = \frac{1}{2\sqrt{2\pi}} (\exp(-(v - \bar{v})^2/2) + \exp(-(v + \bar{v})^2/2)) (1 + \alpha \cos(kx))$$

with parameters  $\alpha = 10^{-3}$ ,  $k = 0.2$ , and  $\bar{v} = 2.4$ . The spatial domain  $D_x = [0, 10\pi]$  as well as the computational domain for velocity  $D_v = [-7, 7]$  is discretized using 128 grid points in each domain. The time step size is  $\Delta t = 10^{-3}$ . As proposed in [12], the truncation strategy uses a truncation tolerance  $\vartheta = 10^{-12}$  to control the energy error. A comparison of the resulting energy when using the continuously conservative BUG and the conservative augmented BUG integrator can be found in Figure 8a which demonstrates an almost identical approximation quality of both integrators. As shown in Figure 8b-d, mass and momentum are conserved up to machine precision for the conservative integrators. The energy error differs for both methods, however, the overall error behavior is similar. Again, the standard augmented BUG integrator fails to conserve momentum and mass up to machine precision. Moreover, the rank shown in Figure 9 is identical for the conservative methods, whereas the standard augmented BUG integrator exhibits slightly lower ranks in comparison.

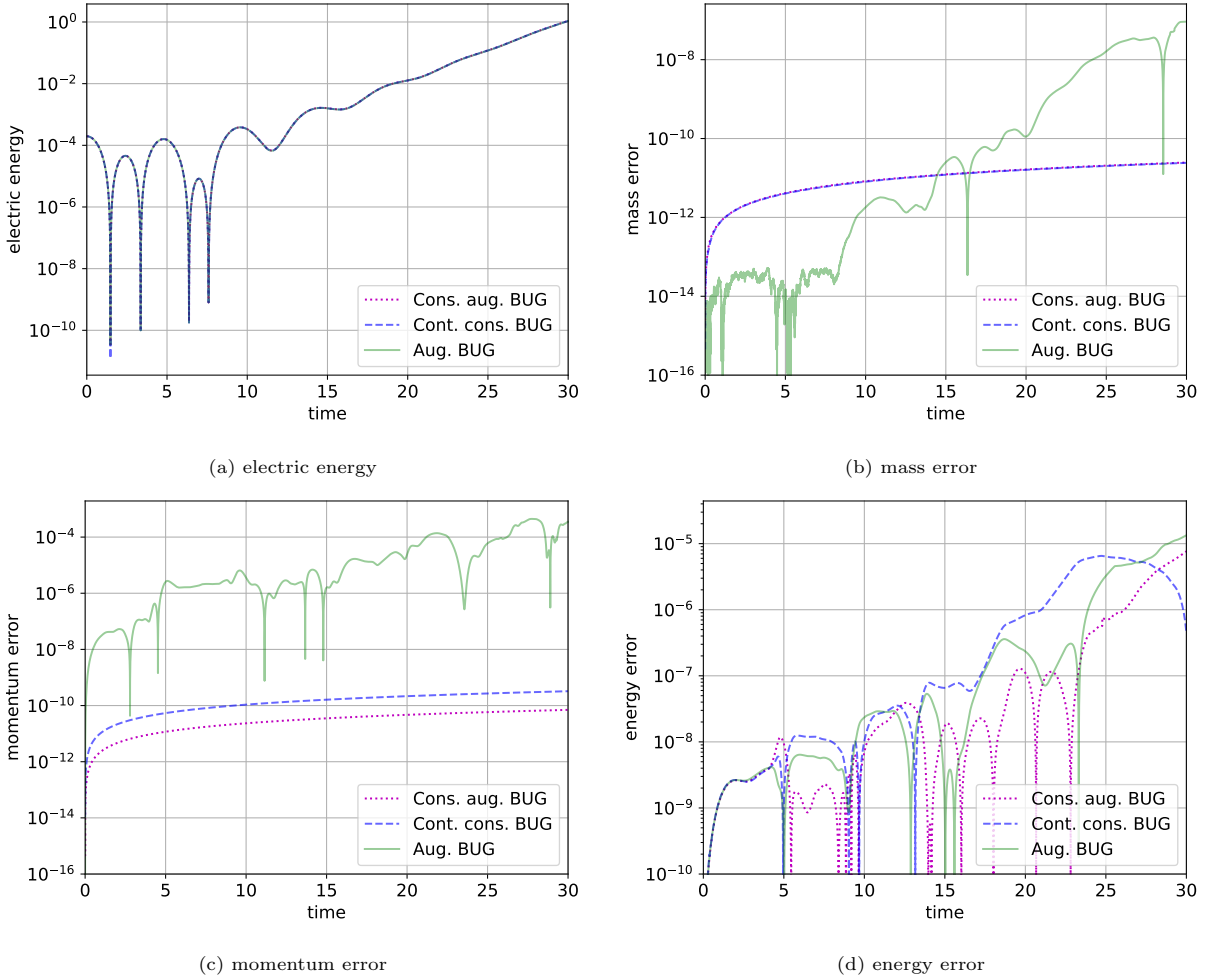


Figure 8: Comparison of the continuously conservative integrator (cont. cons. BUG) of [12], the conservative augmented BUG integrator and the standard augmented BUG integrator of [2] for the two-stream instability test case.  $\vartheta = 10^{-12}$ ,  $t_{\text{end}} = 30$ .

## 6. Conclusion

In the work, we have demonstrated conservation properties of the conservative augmented BUG integrator for kinetic problems. This property is achieved by using a conservative truncation step. The resulting integrator does not require augmenting the basis with additional functions or solving modified evolution equations to preserve basis functions, thereby reducing computational costs. However, we note that using the conservative augmented BUG integrator to solve the conservative system (3) will yield satisfactory results and provide a viable alternative.

## 7. Acknowledgements

The work of Steffen Schotthöfer is sponsored by the Office of Advanced Scientific Computing Research, U.S. Department of Energy, and performed at the Oak Ridge National Laboratory, which is managed by UT-Battelle, LLC under Contract No. DE-AC05-00OR22725 with the U.S. Department of Energy. The United States Government retains and the publisher, by accepting the article for publication, acknowledges that the United States Government retains a non-exclusive, paid-up, irrevocable, world-wide license to publish or reproduce the published form of this manuscript, or allow others to do so, for United States Government



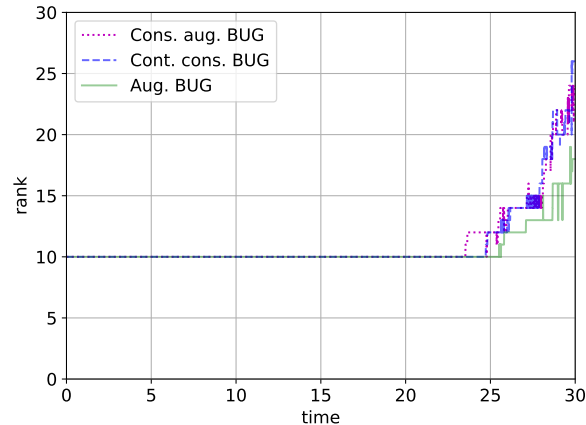


Figure 9: Rank comparison of the continuously conservative integrator (cont. cons. BUG) of [12], the conservative augmented BUG integrator and the standard augmented BUG integrator of [2] for the two-stream instability test case.  $\vartheta = 10^{-12}$ ,  $t_{\text{end}} = 30$ .

purposes. The Department of Energy will provide public access to these results of federally sponsored research in accordance with the DOE Public Access Plan (<http://energy.gov/downloads/doe-public-access-plan>).

## References

- [1] F. Cassini and L. Einkemmer. Efficient 6d vlasov simulation using the dynamical low-rank framework ensign. *Computer Physics Communications*, 280:108489, 2022.
- [2] G. Ceruti, J. Kusch, and C. Lubich. A rank-adaptive robust integrator for dynamical low-rank approximation. *BIT Numerical Mathematics*, pages 1–26, 2022.
- [3] G. Ceruti, J. Kusch, and C. Lubich. A parallel rank-adaptive integrator for dynamical low-rank approximation. *arXiv preprint arXiv:2304.05660*, 2023.
- [4] G. Ceruti and C. Lubich. An unconventional robust integrator for dynamical low-rank approximation. *BIT Numerical Mathematics*, 62(1):23–44, 2022.
- [5] J. Coughlin and J. Hu. Efficient dynamical low-rank approximation for the vlasov-ampère-fokker-planck system. *Journal of Computational Physics*, 470:111590, 2022.
- [6] Z. Ding, L. Einkemmer, and Q. Li. Dynamical low-rank integrator for the linear boltzmann equation: error analysis in the diffusion limit. *SIAM Journal on Numerical Analysis*, 59(4):2254–2285, 2021.
- [7] L. Einkemmer, J. Hu, and J. Kusch. Asymptotic-preserving and energy stable dynamical low-rank approximation. *arXiv preprint arXiv:2212.12012*, 2022.
- [8] L. Einkemmer, J. Hu, and Y. Wang. An asymptotic-preserving dynamical low-rank method for the multi-scale multi-dimensional linear transport equation. *Journal of Computational Physics*, 439:110353, 2021.
- [9] L. Einkemmer and I. Joseph. A mass, momentum, and energy conservative dynamical low-rank scheme for the vlasov equation. *Journal of Computational Physics*, 443:110495, 2021.
- [10] L. Einkemmer and C. Lubich. A low-rank projector-splitting integrator for the vlasov–poisson equation. *SIAM Journal on Scientific Computing*, 40(5):B1330–B1360, 2018.
- [11] L. Einkemmer and C. Lubich. A quasi-conservative dynamical low-rank algorithm for the Vlasov equation. *SIAM Journal on Scientific Computing*, 41(5):B1061–B1081, 2019.
- [12] L. Einkemmer, A. Ostermann, and C. Scalone. A robust and conservative dynamical low-rank algorithm. *Journal of Computational Physics*, 484:112060, 2023.
- [13] B. Ganapol. Homogeneous infinite media time-dependent analytic benchmarks for x-tm transport methods development. *Los Alamos National Laboratory*, 1999.
- [14] B. Ganapol. *Analytical benchmarks for nuclear engineering applications*. 2008.
- [15] W. Guo and J.-M. Qiu. A conservative low rank tensor method for the vlasov dynamics. *arXiv preprint arXiv:2201.10397*, 2022.
- [16] C. D. Hauck and S. Schnake. A predictor-corrector strategy for adaptivity in dynamical low-rank approximations. *SIAM Journal on Matrix Analysis and Applications*, 44(3):971–1005, 2023.
- [17] J. Hu and Y. Wang. An adaptive dynamical low rank method for the nonlinear boltzmann equation. *Journal of Scientific Computing*, 92(2):75, 2022.

- [18] O. Koch and C. Lubich. Dynamical low-rank approximation. *SIAM Journal on Matrix Analysis and Applications*, 29(2):434–454, 2007.
- [19] J. Kusch, L. Einkemmer, and G. Ceruti. On the stability of robust dynamical low-rank approximations for hyperbolic problems. *SIAM Journal on Scientific Computing*, 45(1):A1–A24, 2023.
- [20] Kusch, Jonas and Stammer, Pia. A robust collision source method for rank adaptive dynamical low-rank approximation in radiation therapy. *ESAIM: M2AN*, 57(2):865–891, 2023.
- [21] C. Lubich and I. V. Oseledets. A projector-splitting integrator for dynamical low-rank approximation. *BIT Numerical Mathematics*, 54(1):171–188, 2014.
- [22] Z. Peng and R. G. McClarren. A high-order/low-order (holo) algorithm for preserving conservation in time-dependent low-rank transport calculations. *Journal of Computational Physics*, 447:110672, 2021.
- [23] Z. Peng and R. G. McClarren. A sweep-based low-rank method for the discrete ordinate transport equation. *Journal of Computational Physics*, 473:111748, 2023.
- [24] S. Schotthöfer, E. Zangrando, J. Kusch, G. Ceruti, and F. Tudisco. Low-rank lottery tickets: finding efficient low-rank neural networks via matrix differential equations. In S. Koyejo, S. Mohamed, A. Agarwal, D. Belgrave, K. Cho, and A. Oh, editors, *Advances in Neural Information Processing Systems*, volume 35, pages 20051–20063. Curran Associates, Inc., 2022.
- [25] E. Zangrando, S. Schotthöfer, G. Ceruti, J. Kusch, and F. Tudisco. Rank-adaptive spectral pruning of convolutional layers during training, 2023.